Comprehensive Study of Moisture Risk on Building Facades Based on Spatial Distribution of Wetting and Drying

Xiaohai Zhou, PhD **Aytac Kubilay, PhD**

Dominique Derome, PhD **Jan Carmeliet, PhD**

ABSTRACT

Moisture is one of the main factors affecting the durability of buildings. Moisture conditions within buildings result from their wetting and drying behavior. Wind-driven rain (WDR) is often the largest moisture source for wetting of building envelopes whereas evaporation is the main mechanism that removes water from porous building materials. Moisture-induced damage risk of building envelopes is mostly evaluated with one-dimensional hygrothermal simulations. In these studies, WDR load on building facades is typically estimated with semi-empirical methods, leading to uniform WDR intensity across large parts of facades with large uncertainties. Similarly, the convective moisture transfer coefficient (CMTC), a key parameter for the calculation of evaporation rate, is commonly calculated with simple empirical equations and taken as a surface-averaged value. This simplification underestimates the evaporation rate for regions of the façade that are more exposed to wind and overestimates for those that are less exposed. The balance of WDR load and CMTC determines moisture risk at the different parts of a building façade. The regions with a higher WDR load typically indicate a higher moisture risk whereas the regions with a higher CMTC indicate a lower moisture risk. When the actual spatial distributions of WDR and CMTC are not considered, the moisture risk of facades cannot be accurately evaluated in detail. Additionally, locations with the highest moisture risk cannot be determined. In this study, an integrated model that considers air flow around a building, WDR, radiation, moisture and heat transport in the building envelope is used to analyze moisture risk on a building façade. The spatial distributions of both WDR load and CMTC on the building facade are obtained with computational fluid dynamics (CFD) simulations. There are large spatial variations of WDR and CMTC on the façade. Generally speaking, locations with higher WDR load have also higher CMTC. Therefore, the location with a higher WDR load may not always be the location with a higher moisture risk. The moisture level on the façade is affected by both WDR and CMTC. Both wetting and drying components need to be accurately determined to ensure a reliable evaluation of moisture risk on building facades.

Xiaohai Zhou is a senior scientist at the Chair of Building Physics at ETH Zurich, Zurich, Switzerland. **Aytac Kubilay** is a senior scientist at the Chair of Building Physics at ETH Zurich, Zurich, Switzerland. **Dominique Derome** is a professor at the Department of Civil and Building Engineering, Université de Sherbrooke, Sherbrooke, Canada. **Jan Carmeliet** is a professor at the the Chair of Building Physics at ETH Zurich, Zurich, Switzerland.

INTRODUCTION

Moisture is one of the main factors affecting the durability of buildings. Around 70% of all building problems are estimated to be directly or indirectly related to moisture (Hens, 2017). Too high moisture content in building envelopes can result in moisture-related problems such as mould growth, freeze-thaw damage, wood rot, a decrease in thermal resistance of insulation materials and poor indoor air quality. The moisture condition of building envelopes is affected by both wetting and drying processes. Wind-driven rain (WDR) is the largest wetting source that affects the hygrothermal performance of building envelopes. The drying process mainly occurs with the evaporation of water from porous building materials to the surrounding air. Zhou et al. (2016) developed the Climatic Index which considers WDR as wetting component and potential evaporaton as drying component to indicate the risk of moisture problems of building envelopes in different climates.

Hygrothermal models, which simulate coupled moisture and heat transport in building envelopes, are used for assessing the moisture performance of wall envelopes. In the past, they have been used to study the influences of internal thermal insulation (Zhou et al. 2020a; Zhou et al. 2022), rainwater leakage (Künzel and Zirkelbach, 2013), cavity ventilation (Künzel et al., 2008), climate change (Nik et al., 2015; Sehizadeh and Ge 2016; Zhou et al. 2020b) and wall papers (Ryu et al. 2015), and many others, on the risk of moisture-related problems of building envelopes. Moisture risk of building envelopes is mostly evaluated with one-dimensional hygrothermal simulations. In most hygrothermal studies, WDR load on building facades is estimated with semi-empirical methods, which is considered uniform across large parts of facades with large uncertainties. The convective moisture transfer coefficient (CMTC), a key parameter for the calculation of evaporation from building envelope, is commonly calculated based on Lewis analogy with convective heat transfer coefficient (CHTC) and is a surface-averaged value. The 1D hygrothermal simulations result in a very large uncertainty on the analysis of moisture risk on building façade. Besides, there is no reliable data on the distribution of moisture risk at the different locations of the building façade. Therefore, it is not known which location on the building façade has the highest moisture risk. As a result, the same moisture protection measures are often applied to the entire building façade.

In this study, an integrated model that considers air flow around buildings, WDR, radiation, moisture and heat transport in the building envelope is used to analyze moisture risk on a building façade. The moisture risk at the different locations of the building façade is analyzed based on the spatial distribution of both WDR load and CMTC on the façade, which are obtained with computational fluid dynamics (CFD) simulations.

NUMERICAL MODEL

The integrated model has four parts: (1) a CFD model which simulates air, heat and moisture transport in the air domain; (2) a WDR model which simulates WDR load on building facades; (3) a hygrothermal model which simulates coupled heat and moisture transport in porous building materials; (4) a radiation model which simulates shortwave and longwave radiation exchange between the building surfaces, the surrounding environment and the sky. A detailed description of the integrated model can be found in Kubilay et al. (2018) and Ferrari et al. (2020).

Computational fluid dynamics (CFD) model

The wind flow is simulated by the 3D Steady RANS (Reynolds-Averaged Navier-Stokes) with the standard k-ε model for turbulence. In addition, governing equations for heat transport (modeled as an active scalar) and moisture transport (modeled as a passive scalar) in the air domain are solved. The governing equations are described with a compressible formulation of the Navier-Stokes equations. Mass, momentum and energy conservation equations for dry air are given as:

$$\frac{\partial \rho_a}{\partial t} + \nabla \cdot (\rho_a \boldsymbol{u}) = 0 \tag{1}$$

$$\frac{\partial (\rho_a \boldsymbol{u})}{\partial t} + \nabla \cdot (\rho_a \boldsymbol{u}\boldsymbol{u}) = -\nabla p_a - \nabla \cdot \tau + \rho_a \boldsymbol{g} \tag{2}$$

$$\frac{\partial (\rho_a h_a)}{\partial t} + \frac{\partial (\rho_a K_a)}{\partial t} + \nabla \cdot (\rho_a h_a \boldsymbol{u}) + \nabla \cdot (\rho_a K_a \boldsymbol{u}) = -\nabla \cdot \boldsymbol{q} \tag{3}$$

where ρ_a is the density of dry air, $\boldsymbol{u}$ is the air velocity, p_a is the air pressure, τ is the viscous stress tensor, $\boldsymbol{g}$ is the gravity, h_a is the specific enthalpy, K_a (=0.5u^2) is the specific kinetic energy, $\boldsymbol{q}$ is the heat flux. The standard k-ε model is used to model

Reynolds stresses, turbulent kinetic energy, turbulent viscosity and turbulent dissipation (Launder and Sharma, 1974). The heat flux $\boldsymbol{q}$ in Eq. 3 is written as:

$$\boldsymbol{q} = -\lambda_{eff}\nabla T = -(\lambda_a + \frac{C_{p,a}\mu_t}{\mathrm{Pr}_t})\nabla T \tag{4}$$

where λ_a is the thermal conductivity of dry air, Pr_t is the turbulent Prandtl number, μ_t is the turbulent viscosity.
It is assumed that air consists of dry air and water vapor. Vapor transport in the air is decoupled from dry air transport. The mass conservation equation for moisture in the air is given as:

$$\frac{\partial \rho_v}{\partial t} + \nabla \cdot (\rho_v \boldsymbol{u}) = -\nabla \cdot g_{d,v} \tag{5}$$

where ρ_v is the vapor density, $g_{d,v}$ is the diffusive vapor flux, described by Fick's law as:

$$g_{d,v} = -\rho_a D_{va,eff} \nabla \frac{\rho_v}{\rho_a} \tag{6}$$

where $D_{va,eff}$ is the effective diffusion coefficient. It is defined as the sum of the vapor diffusion coefficient and turbulent diffusion coefficient:

$$D_{va,eff} = D_{va} + \frac{\mu_t}{\rho_g Sc_t} \tag{7}$$

where D_{va} is the vapor diffusion coefficient in air and Sc_t is the turbulent Schmidt number.
The amount of moisture in the air can be described with humidity ratio, w, as:

$$w = \frac{\rho_v}{\rho_a} = \frac{p_v}{R_v T}\frac{R_a T}{p_a} = \frac{R_a}{R_v}\frac{\phi p_{v,sat}}{p_a} \tag{8}$$

where p_v is the partial vapor pressure, R_v is the gas constant of vapor, Φ is the relative humidity, $p_{v,sat}$ is the saturated vapor pressure.
The mass conservation equation for moisture in the air can be written with humidity ratio as the dependent variable:

$$\frac{\partial \rho_a w}{\partial t} + \nabla \cdot (\rho_a w \boldsymbol{u}) = \nabla \cdot (\rho_a D_{va,eff} \nabla w) \tag{9}$$

Wind-driven rain (WDR) model

An Eulerian multiphase (EM) model is used for the simulation of WDR. In the EM model, the rain phase is also viewed as a continuum, similar to air flow. Each class of raindrop sizes is treated as a different rain phase as each group of raindrops of similar size interacts with the wind flow field in a similar way. Rain phase calculations are one-way coupled with the air phase. The calculated wind flow field is used for driving the raindrops in the rain simulations and the influence of raindrops on the wind flow is neglected. The WDR model has been validated by several field measurement studies (Kubilay et al. 2013, 2014, 2015).
The WDR load on building surface is calculated based on horizontal rainfall intensity (R_h) and catch ratio (η):

$$R_{WDR} = R_h \eta \tag{10}$$

The catch ratio η is related to specific catch ratio $\eta_d(d)$ and raindrop size distribution through a horizontal plane $f_h(d)$:

$$\eta = \int_d f_h(d)\eta_d(d)\mathrm{d}d \tag{11}$$

The distribution of specific catch ratio $\eta_d(d)$ for each rain phase is calculated with the following equation:

$$\eta_d(d) = \frac{R_{WDR}(d)}{R_h(d)} = \frac{\alpha_d |V_n(d)|}{R_h f_h(R_h, d)} \tag{12}$$

where $R_{WDR}(d)$ is WDR intensity of the rain phase with the diameter of d, $R_h(d)$ is the horizontal rainfall intensity of the rain phase with the diameter of d, $|Vn(d)|$ is the velocity magnitude of the rain phase with the diameter d in the direction normal to the building surface.

Hygrothermal model for transport in building envelopes

Moisture and heat transport in the building envelopes is simulated with the hygrothermal model which solves conservation equations for moisture and energy. A porous building material consists of solid matrix and pores. Moisture exists in the pores in the form of liquid water and vapor. The Kelvin equation is used to describe the thermodynamic equilibrium between the liquid phase and the vapor phase. A detailed description of the hygrothermal model can be found in Janssen et al. (2007) . The governing equations for moisture and heat transport within the porous building materials are given in Eq. 13 and 14, respectively, where g_l and g_v represent liquid (Eq. 15) and vapor (Eq. 16) flow rates.

$$\frac{\partial w}{\partial p_c}\frac{\partial p_c}{\partial t} + \nabla \cdot (\mathrm{g}_l + \mathrm{g}_v) = 0 \tag{13}$$

$$(c_0 \cdot \rho_0 + c_l \cdot w) \cdot \frac{\partial T}{\partial t} + \nabla \cdot (c_l \cdot (\mathrm{T} - \mathrm{T}_{ref}) \cdot g_l + (c_v \cdot (\mathrm{T} - \mathrm{T}_{ref}) + L_v) \cdot g_v) = -\nabla(\lambda \nabla T) \tag{14}$$

$$g_l = -K_l \cdot \nabla p_c \tag{15}$$

$$g_v = -\delta_v \cdot \frac{p_v}{\rho_l \cdot R_v \cdot T} \cdot \nabla p_c - \delta_v \cdot \frac{p_v}{\rho_l \cdot R_v \cdot T^2} (\rho_l \cdot L_v) \cdot \nabla T \tag{16}$$

where w is the moisture content, p_c is the capillary pressure, K_l is the liquid permeability of porous building materials, δ_v is the water vapor permeability of porous building materials, p_v is the vapor pressure, ρ_l is the density of water, R_v is the gas constant of water vapor, T is the absolute temperature, c_0 is the specific heat capacity of dry solid (J/kg K), c_l is the specific heat capacity of liquid water (J/kg K), c_v is the specific heat capacity of vapor (J/kg K), ρ_0 is the density of dry solid (kg/m3), T_{ref} is the reference temperature (273.15 K), L_v is the latent heat of vaporization (J/kg), λ is the thermal conductivity (W/mK). The hygrothermal model has been verified against HAMSTAD benchmarks (Hagentoft et al. 2004; Ferrari et al. 2020).

The moisture flux at the exterior surfaces of building envelopes, g_{ext} consists of two parts: the convective vapor flux (g_{conv}) and the WDR flux (R_{wdr}), as is shown in Eq. 17. $p_{v,a}$ is the vapor pressure of the air near wall envelope and $p_{v,w}$ is the vapor pressure of wall surface. The heat flux consists of convective heat flux (q_{conv}), sensible heat flux due to rain (R_s), radiative heat flux (S), and sensible and latent heat flux due to the vapor flux (q_{ls}), as is shown in Eq. 18.

$$g_{ext} = g_{conv} + R_{wdr} = CMTC \cdot (p_{v,a} - p_{v,w}) + R_{wdr} \tag{17}$$

$$q_{ext} = q_{conv} + R_s + S + q_{ls} \tag{18}$$

$$q_{ls} = (c_v \cdot (\mathrm{T} - \mathrm{T}_{ref}) + L_v) \cdot g_{conv} \tag{19}$$

The convective moisture and heat fluxes at the exterior surfaces of the building envelopes are obtained from the CFD calculation in the air domain. The WDR flux is calculated from the WDR model.

Radiation model

The radiation model calculates the shortwave and longwave radiation exchange between the building surfaces, the ground and the sky. The radiation exchange is calculated based on a radiosity approach with view factors. Air is considered as a non-participating medium. Therefore, absorption, scattering and emission of radiation by air are neglected. It is assumed that all surfaces are opaque and thus transmissivity on surfaces is zero. Building and ground surfaces are assumed to be gray and diffuse and therefore absorptivity and emissivity on the surfaces are equal and independent of direction and wavelength.

Solution algorithm

The integrated model is implemented in OpenFOAM (windDrivenRainFoam and urbanMicroclimateFoam). The WDR load on the building façade is obtained separately with the WDR model and used as boundary condition for simulation in the building envelopes. The coupling between the air and building envelopes is achieved by solving governing equations in the air and governing equations in the building envelopes for each exchange timestep in sequence. The exchange time step is defined as the time at which data are exchanged at the boundaries between the air and building envelopes. The exchange time step is selected to be 1 hour, which is accurate enough for the analysis of moisture risk on buildings, as the moisture risk is related to long-term wetting and drying behavior.

For each exchange time step, the steady air flow is first solved. The Semi-Implicit Method for Pressure Linked Equations (SIMPLE) algorithm is used for pressure-velocity coupling. The simulation continues until all scaled residuals are below the specified tolerances: 10^{-5} for all velocity components, pressure, and turbulent terms, 10^{-4} for heat and humidity ratio. Then

the computed moisture and heat flux at the air-building interface are used as boundary conditions for moisture and heat simulation in the building envelopes. The transient moisture and heat transport in the building envelopes are simulated using adaptive timesteps. For each timestep, capillary pressure and temperature are updated until Picard residuals become smaller than a given tolerance. Finally, the calculated moisture content and temperature at the air-building interface are applied to solve the steady air flow for the next exchange timestep. The majority of the computing time is used for CFD calculations in the air.

CASE STUDY

This paper studies the influence of wetting and drying on moisture distribution on a building facade in Zurich, Switzerland. A pitched building with the dimension of length × width × height of 10 × 10 × 10 m^3 is used for study (Fig. 1a). The facades of the building are facing exactly north, south, east and west. This study focuses on the west-facing façade, as this façade orientation has the highest WDR load in Zurich. The slope of the roof is 30.0° and the length of the overhang at the west-facing façade is 1.0 m.

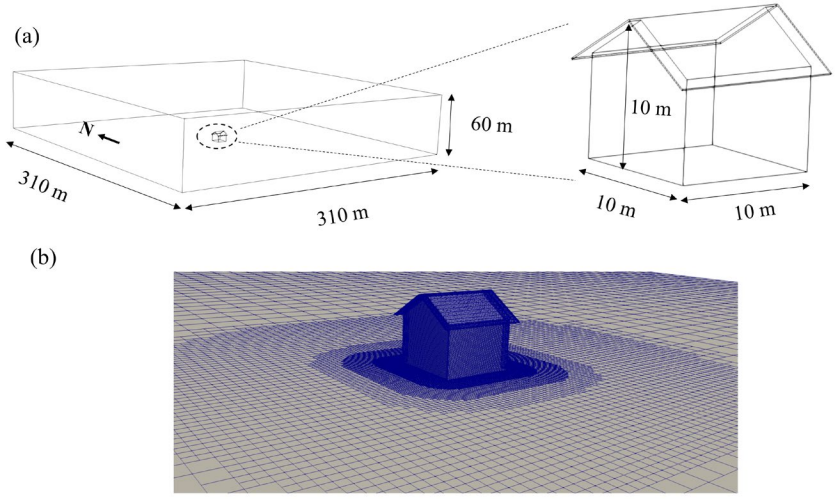

Figure 1 (a) Computational domain of the case study and (b) computational cells for air domain showing the building surfaces and part of the ground.

Calculation domain for air

The extent of the calculation domain has a size of 310 × 310 × 60 m^3 (Fig. 1a). The distance of the building to the boundaries in the lateral and vertical directions meets the guidelines presented in Franke et al (Franke et al. 2007). The total number of cells in the computational grid for air is 1’847’938. Parts of the grid on the ground and building surfaces are shown in Fig. 1b. The cells are progressively refined towards the wall boundary to properly capture the gradient at the wall. For building and ground surfaces, standard wall functions are used (Launder and Sharma 1974). The inlet is selected based on wind direction. For example, when the wind comes from the southwest, the south and west surfaces of the calculation domain are selected as inlet and the north and east surfaces of the calculation domain are selected as outlet. At the inlet boundary, the vertical profiles of velocity, turbulent kinetic energy and dissipation are given according to the atmospheric boundary layer profile considering neutral conditions (Richards and Hoxey 1993). At the outlet boundary, a constant static gauge pressure of 0.0 Pa is applied.

Calculation domain for building facade

Moisture and heat transport at the westing-facing facade is simulated. The wall envelope considered is an internally insulated

masonry wall, consisting of brick, mortar, plaster, glass wool and vapor barrier (Fig. 2b). First, the façade surface is discretized into 8829 triangular cells (Fig. 2a). Then, the surface mesh is extruded in the normal direction to create the 3D mesh of the wall envelope, as shown in Fig. 2c. The mesh is refined at the interfaces between each material. In total, the calculation domain of the façade consists of 4'414'500 cells. The boundary conditions at the exterior surface are set according to Eq. 14 and 15. The indoor conditions are calculated according to the European standard EN15026, in which indoor air temperature and relative humidity depend linearly on the outdoor temperature. The initial conditions of the building envelope are at uniform temperature of 20 °C and relative humidity of 60%.

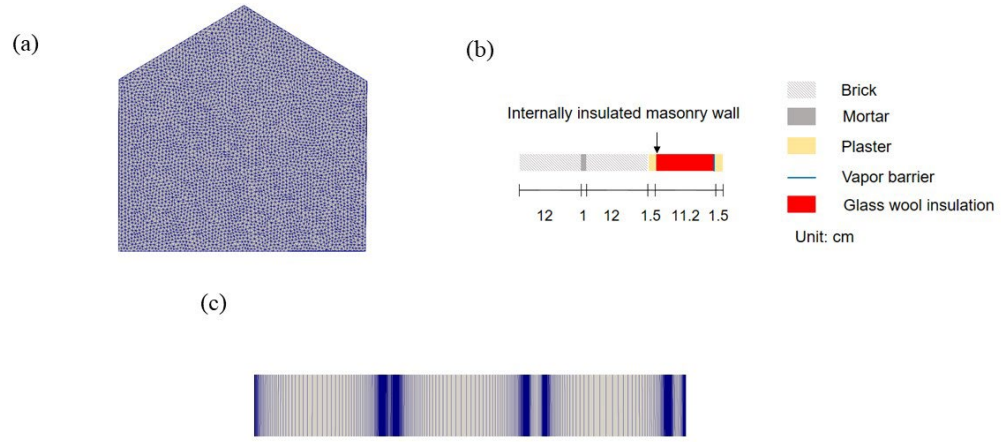

Figure 2 (a) Discretization of the west-facing façade; (b) geometry and building materials along the thickness of the wall envelope and (c) discretization along the thickness of the wall envelope.

Meteorological conditions

A meteorological data of 50 days from 1st October 2003 to 20st November 2003 at Zurich Kloten weather station is used as input. The meteorological data include hourly horizontal rainfall, global solar radiation, air temperature and relative humidity, wind speed and direction.

RESULTS

The numerical simulations of WDR are carried out for 12 wind directions with 30° steps from 0° to 360° and 6 wind speeds (1, 3, 5, 7, 10 and 20 m/s). For each wind speed, specific catch ratio distributions are calculated for 17 raindrop diameters in the range from 0.3 to 6 mm. Fig. 3a shows the distribution of the mean catch ratio on the west-facing façade for the total calculation period of 50 days with a total amount of horizontal rainfall of 189.4 mm. The WDR load on the building façade is equal to the amount of the horizontal rainfall multiplied by the catch ratio. The upper part of the façade is well protected by the overhang, where the catch ratio is mostly smaller than 0.12. The catch ratio is much larger at the right (southern) edge and ranges between 0.15 and 0.20. Compared to the right edge, the catch ratio is much smaller and ranges between 0.12 and 0.15 at the left (northern) edge. The smaller catch ratio at the left edge is mainly due to the predominant wind direction during rainfall in Zurich, which is west-southwest. The lower part of the façade has a catch ratio of around 0.09. Fig. 3b shows the mean CMTC at the west-facing facade in the calculation period. In general, the lateral parts show larger CMTC than the upper and lower parts. The CMTC ranges between 6.0e-8 to 8.0e-8 s/m at the lateral parts while it ranges between 3.0e-8 and 5.0e-8 s/m at the top and lower parts. Considering the distribution of catch ratio and CMTC, the lateral parts of the facade are exposed to both larger wetting and drying components while the upper and lower parts are exposed to both smaller wetting and drying components.

Fig. 4 shows the distribution of relative humidity at the interface between plaster and glass wool insulation after 50 days. The interface between plaster and glass wool insulation is the most critical location in the case of an internally insulated wall envelope. The RH at the interface is between 0.87 and 0.95. The largest relative humidity is at the lower part of the right edge

and the lowest RH is at the uppermost part of the façade (location D). Although the WDR load at the middle part of the right edge (e.g. location A) is larger than the middle part of the façade (e.g. location B), the larger CMTC at the middle part of the right edge leads to smaller RH at this location. In general, the difference in relative humidity in the middle and lower part of the façade is quite small. The overhang of the building results in low relative humidity at the upper part of the façade. The WDR load at location E is much smaller than that at locations A, B and C while the CMTC at location E is also much smaller than at locations A, B and C (Table 1). However, due to the combined influence of wetting and drying components, relative humidity at location E is only slightly different from RH at locations A, B and C (Table 1). The change in RH at the interface between plaster and glass wool insulation at the different locations over the simulation period is shown in Fig. 5a. In general, RH at the different locations presents a similar trend with increasing values. Due to almost no WDR load at location D, the RH at this location is mostly smaller than the other locations. After 30 days, RH at locations A, B, C, and E still show an increasing trend where RH at location D levels off. The difference in relative humidity at locations A, B, C and E is rather small. The RH profiles of the wall envelope at locations A, B, C, D and E at the 50th day are shown in Fig. 5b. The RH profile at location D shows much lower values compared to the other locations. The mean CMTCs are almost the same at locations A and C. However, the larger WDR load at location A leads to a higher RH profile at location A. Although locations A and B have quite different WDR and CMTC, the RH profiles at these two locations are almost the same. It can be seen that both the wetting component and drying component have a large influence on the moisture level in the wall envelope.

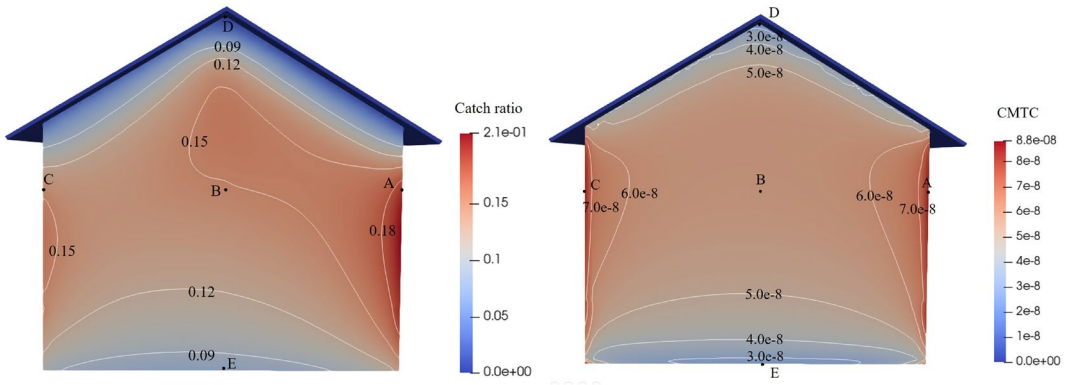

Figure 3 (a) Mean catch ratio (-) at the west-facing facade in the calculation period; (b) mean CMTC (s/m) at the west-facing facade in the calculation period.

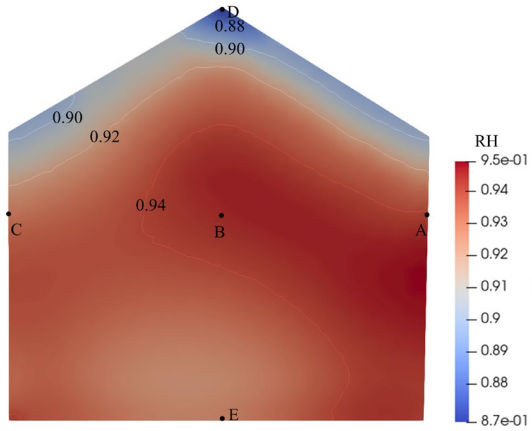

Figure 4 Distribution of relative humidity (-) at the interface between plaster and glass wool insulation after 50 days.

Table 1. WDR catch ratio, CMTC and RH at the 5 locations

Location	WDR catch ratio (-)	CMTC (s/m)	RH at 50th day (-)
A	0.176	8.50e-8	0.942
B	0.132	5.69e-8	0.945
C	0.125	8.31e-8	0.928
D	0.003	2.35e-8	0.868
E	0.069	2.83e-8	0.926

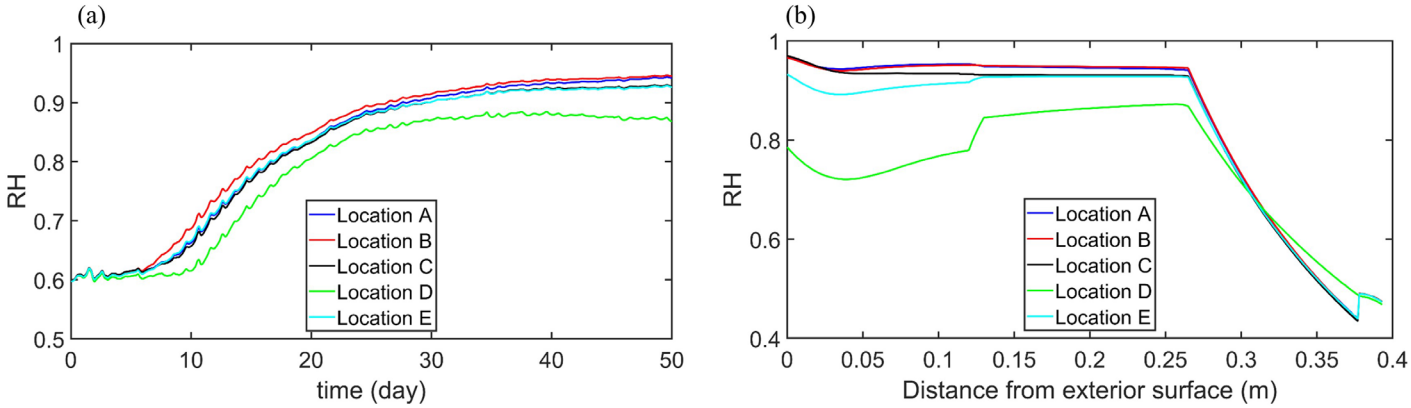

Figure 5 (a) Time-series result of RH at the interface between plaster and glass wool insulation at the different locations (the interface between plaster and glass wool insulation is shown with an arrow in Fig. 2b); (b) RH profile along the thickness of the wall envelope at the different locations after 50 days.

CONCLUSION

An integrated model that considers air flow, radiation, moisture and heat transport in the building envelope is used to study moisture risk on a building façade. The spatial distributions of both WDR load and CMTC on the building facade are analyzed. In general, the location which has a high WDR load presents also a high value of CMTC. The combined influence of WDR and CMTC determines the moisture level in a building envelope. Due to the large difference in the distribution of WDR and CMTC on the building facade, moisture risk at the different locations can also be quite different. Both the wetting component and drying component have a large influence on the moisture level in the wall envelope. A location with a high WDR load may not always be the location with a high moisture risk. A location with a low WDR could have a high moisture risk when CMTC is also considerably low. Therefore, wetting and drying components need to be accurately determined to ensure a reliable evaluation of moisture risk on building facades.

ACKNOWLEDGEMENT

Andreas Rubin is acknowledged for his help with the STL file of the building. We would like to thank MeteoSwiss for providing the meteorological data.

REFERENCES

Franke, J., Hellsten, A., Schlünzen, K.H., Carissimo, B., 2007. Best practice guideline for the CFD simulation of flows in the urban environment-a summary, in: *11th Conference on Harmonisation within Atmospheric Dispersion Modelling for Regulatory Purposes*, Cambridge, UK, July 2007. Cambridge Environmental Research Consultants.

Ferrari, A., Kubilay, A., Derome, D., Carmeliet, J., 2020. The use of permeable and reflective pavements as a potential strategy for urban heat island mitigation. *Urban Climate* 31, 100534.

Hagentoft, C.-E., Kalagasidis, A.S., Adl-Zarrabi, B., Roels, S., Carmeliet, J., Hens, H., Grunewald, J., Funk, M., Becker, R., Shamir, D., 2004. Assessment method of numerical prediction models for combined heat, air and moisture transfer in building components: benchmarks for one-dimensional cases. *Journal of thermal envelope and building science* 27, 327–352.

Hens, H.S.L., 2017. *Building physics-heat, air and moisture: fundamentals and engineering methods with examples and exercises*. John Wiley & Sons.

Janssen, H., Blocken, B., Carmeliet, J., 2007. Conservative modelling of the moisture and heat transfer in building components under atmospheric excitation. *International Journal of Heat and Mass Transfer* 50, 1128–1140.

Kubilay, A., Derome, D., Blocken, B., Carmeliet, J., 2015. Wind-driven rain on two parallel wide buildings: field measurements and CFD simulations. *Journal of Wind Engineering and Industrial Aerodynamics* 146, 11–28.

Kubilay, A., Derome, D., Blocken, B., Carmeliet, J., 2014. Numerical simulations of wind-driven rain on an array of low-rise cubic buildings and validation by field measurements. *Building and environment* 81, 283–295.

Kubilay, A., Derome, D., Blocken, B., Carmeliet, J., 2013. CFD simulation and validation of wind-driven rain on a building facade with an Eulerian multiphase model. *Building and environment* 61, 69–81.

Kubilay, A., Derome, D., Carmeliet, J., 2018. Coupling of physical phenomena in urban microclimate: A model integrating air flow, wind-driven rain, radiation and transport in building materials. *Urban climate* 24, 398–418.

Künzel, H.M., Karagiozis, A.N., Kehrer, M., 2008. Assessing the benefits of cavity ventilation by hygrothermal simulation, in: *Building Physics Symposium in Honour of Prof. Hugo LSC Hens*. Leuven, Belgium.

Künzel, H.M., Zirkelbach, D., 2013. Advances in hygrothermal building component simulation: modelling moisture sources likely to occur due to rainwater leakage. *Journal of Building Performance Simulation* 6, 346–353.

Launder, B.E., Sharma, B.I., 1974. Application of the energy-dissipation model of turbulence to the calculation of flow near a spinning disc. *Letters in heat and mass transfer* 1, 131–137.

Nik, V.M., Mundt-Petersen, S.O., Kalagasidis, A.S., De Wilde, P., 2015. Future moisture loads for building facades in Sweden: Climate change and wind-driven rain. *Building and Environment* 93, 362–375.

Richards, P.J., Hoxey, R.P., 1993. Appropriate boundary conditions for computational wind engineering models using the k-ϵ turbulence model. *Journal of wind engineering and industrial aerodynamics* 46, 145–153.

Ryu, S.H., Moon, H.J., Kim, J.T., 2015. Evaluation of the influence of hygric properties of wallpapers on mould growth rates using hygrothermal simulation. *Energy and Buildings* 98, 113–118.

Sehizadeh, A., Ge, H., 2016. Impact of future climates on the durability of typical residential wall assemblies retrofitted to the PassiveHaus for the Eastern Canada region. *Building and Environment* 97, 111–125.

urbanMicroclimateFoam — An open-source solver for coupled physical processes modeling urban microclimate based on OpenFOAM. Available online: https://gitlab.ethz.ch/openfoam-cbp/solvers/urbanmicroclimatefoam

windDrivenRainFoam — An Open-Source Solver for Wind-Driven Rain Based on OpenFOAM. Available online: https://gitlab.ethz.ch/openfoam-cbp/solvers/winddrivenrainfoam

Zhou, X., Derome, D., Carmeliet, J., 2016. Robust moisture reference year methodology for hygrothermal simulations. *Building and Environment* 110, 23–35.

Zhou, X., Carmeliet, J., Derome, D., 2020a. Assessment of moisture risk of wooden beam embedded in internally insulated masonry walls with 2D and 3D models. *Building and Environment* 107460.

Zhou, X., Carmeliet, J., Derome, D., 2020b. Assessment of risk of freeze-thaw damage in internally insulated masonry in a changing climate. *Building and Environment* 106773.

Zhou, X., Derome, D., Carmeliet, J., 2022. Analysis of moisture risk in internally insulated masonry walls. *Building and Environment* 212.